

Polymorphic fingerprint as an approach to authenticate Iberian pig categories

Laura Bayes-Garcia¹, Eduard Colomer-Llombart¹, Mercedes Aguilar-Jiménez¹, and Maria Teresa Calvet¹

¹Universitat de Barcelona

May 7, 2020

Abstract

High-commercial-value products are often susceptible to food fraud. Among them, Iberian dry-cured ham is highly appreciated due to its particular and sensory, but also nutritional, properties. There are four different Iberian ham categories (namely bellota, recebo, cebo de campo and cebo), which depend on the rearing system of the pig during the last stage of the fattening phase. However, there is still a lack of a normalized and robust method capable of authenticating the different product categories and, therefore, preventing mislabeling. In this work, we characterized the polymorphism of eighty raw lipid extracts belonging to the four categories of Iberian pig by using DSC and synchrotron radiation XRD techniques. The results showed that bellota and recebo samples exhibited essentially the same crystallization and polymorphic behavior and this was significantly distinguishable from that of cebo de campo and cebo categories. Crystallization and melting temperatures of bellota and recebo samples were significantly lower than those of cebo de campo and cebo, due to its more unsaturated fatty acids composition. Furthermore, lower amount of polymorphic forms was detected in bellota and recebo. By considering the differences in rearing systems of the pigs, we concluded that the key factor which determined the polymorphic behavior of Iberian pig lipid extracts was not the physical exercise practiced by the pig, but the inclusion of acorns in the feeding system. This work demonstrated that crystallographic techniques, like DSC and XRD, may be promoted to be used as fingerprinting tools for the authentication of high-value food products.

1. INTRODUCTION

The problem of food adulteration is by no means a contemporary phenomenon and is likely to be as old as the food processing and production systems themselves (Ellis, et al., 2012). Authentication of food products is of primary importance for consumers and industries at all levels of the production chain. The adulteration of food products normally becomes a means for fraudulent economic gain, as fraudulent actions are commonly applied to high-commercial-value products or to those which are produced in high tonnage. Food products, such as jam, fruit juice, meat, honey, milk, wine or vegetable oils are often adulterated with the addition of cheaper products, dilution processes or mislabeling (Cordella et al., 2002). Nevertheless, the detection of adulterations or the discrimination between different product categories become a very complicated issue when chemical compositions are similar.

Several methodologies have been used for foods authentication, such as spectroscopic techniques, methods based on mass spectrometry, chromatography or calorimetry. Characteristics of spectroscopic techniques are their rapidity and portability, and they can provide the fingerprint of a food product. On the other hand, calorimetric techniques, such as differential scanning calorimetry (DSC), are also rapid and highly sensible, and they can show the authenticity of a food product or the effect of an adulteration on the physicochemical properties of the sample (Chiavaro et al., 2008a and 2008b).

Among high-commercial-value products, traditional Spanish Iberian dry-cured ham is greatly appreciated

for its particular and intense sensorial characteristics and associated with top quality gastronomy worldwide. Mainly produced in the southwest regions of Spain, Iberian pigs (pure breed or crossed with Duroc) are raised according to different systems, so that their dry-cured products are classified into different commercial categories. Four are the categories of Iberian pigs, namely *bellota*, *recebo*, *cebo de campo* and *cebo*. Although according to the current Spanish legislation (Royal Decree 4/2014), *recebo* category has been eliminated and, therefore, nowadays three are the existing categories (*bellota*, *cebo de campo* and *cebo*), it is of primary importance to characterize all of them in order to find a robust method to authenticate the product and prevent fraudulent practices. Regarding the rearing systems which define each Iberian pig category, Table 1 summarizes their characteristics and requirements.

Bellota products, which are the most appreciated and those of highest commercial value, come from pigs with a final fattening period in oak forests (period called *montanera*) during which they exclusively eat acorns, grass and other natural resources. Then, the minimum duration of this period is 60 days and the minimum weight gain of the pig must be of 46 kg. *Recebo* products are obtained from pigs that combine the consumption of acorn and grass with a supplementation of concentrated feeds (minimum duration of *montanera*: 60 days; minimum weight gain: 29 kg). By contrast, *cebo de campo* and *cebo* products come from pigs fed with commercial feeds throughout their life. However, in the case of *cebo de campo*, pigs roam in pasture for at least 60 days prior to slaughter, although they keep eating mainly commercial feeds. The differences in animal nutrition in the final stage of the fattening period may determine the sensory quality of final products, due to different lipid deposition in adipose tissue and intramuscular fat (Tejeda et al., 2002).

Several methods have been used to discriminate among different Iberian dry-cured ham of different categories. Almost all the procedures are based on fat properties, such as melting and slip point, or fatty acid profiles. These methods rely on the fact that *bellota* usually contains higher amounts of oleic acid than other categories (Ruiz et al., 1998). By contrast, other methods include the determination of hydrocarbons (Narváez-Rivas et al., 2008) and volatile compounds profiles (Timón et al., 2001; Narváez-Rivas et al., 2011). Moreover, isotope analyses on the adipose tissue of the animals have also been applied to characterize and differentiate Iberian pork meat as a function of the diet of the animal (González-Martín et al., 1999). As to spectrometric techniques, near-infrared spectrometry (NIR) has also been applied with the same purpose (Arce et al., 2009), although this method could not perfectly discriminate among the different pig categories. Recently, more attention has been paid to the determination of the TAGs composition, as analyses become easier and faster, avoiding the use of saponification and the formation of methyl esters (Díaz et al., 1996; Gallardo et al., 2012). The TAGs composition has been also applied to elucidate the effect of genotype (Tejeda et al., 2002; Petrón et al., 2004; Viera-Alcaide et al., 2008). However, there are still some ambiguities in the results obtained by the methods used until now when high amounts of samples have been analyzed. Although the purpose of the new Spanish regulation consists of protecting the purity of Iberian pig, controlling the breeding and feeding and properly labelling the final product, there is still a lack of a normalized and robust method to discriminate among the different categories.

Some studies have focused on the characterization of physical properties of pork fat. Svenstrup et al. (2005) analyzed the influence of changing the cooling and reheating rates applied to pork fat. By using DSC and XRD techniques, they characterized samples of lard (pork dorsal fat) and leaf pork fat (surrounding the kidneys) in their raw state, their extracted fat fraction, and in liver pâté. The crystallization behavior observed permitted defining the textural properties obtained when pork fats were used in liver pâté. Campos et al. (2002) also applied different cooling rates to lard samples, but in order to observe the effects of such variations on the hardness of fat crystal networks. By contrast, Davenel et al. (1999) studied solid fat content variations of pig adipose tissues in relation to their lipid composition. As to spectroscopic techniques, Raman spectrometry has been applied *in situ* to analyze the crystalline states of fat in porcine adipose tissue (Motoyama et al., 2013). The purpose was to establish a tool for routine monitoring the physical conditions of meat carcasses in refrigerators. The same technique was also proposed to discriminate between pork and beef fat, by analyzing the polymorphic features of the characterized samples (Motoyama et al., 2010).

Our group has recently analyzed the polymorphic behavior of the two most differentiated categories of

Iberian dry-cured ham (*bellota* and *cebo*), and obtained very promising results (Bayés-García et al., 2016), as significant differences, related to the polymorphic behavior of the samples, were detected and permitted to clearly discriminate among the two categories. Crystallographic techniques, such as differential scanning calorimetry (DSC) and X-ray diffraction (XRD, with both laboratory-scale or synchrotron radiation source) have been widely used to study the polymorphism of lipid systems, in order to characterize their physical properties, such as melting, morphology, rheology and texture (Larsson et al., 2006; Bayés-García et al., 2020). Nevertheless, these techniques have been rarely used in food authentication.

In the present work we used DSC and XRD techniques to study the polymorphic behavior of the four Iberian pork categories, including intermediate *recebo* and *cebo de campo* to make a step further. Moreover, we used raw lipid samples, obtained before the curing of the ham, in order to define a more robust method, as curing becomes a very complex procedure in which it is not possible to control the variables which may modify the behavior of the samples. This study demonstrates that crystallographic tools may be promoted in the food authentication field to combat food fraud.

2. MATERIALS AND METHODS

Samples of subcutaneous adipose tissue removed from the coccyx of Iberian pigs were obtained from the Instituto Nacional de Investigación y Tecnología Agraria y Alimentaria (INIA) (Zafra, Spain). Lipid fractions were extracted and dehydrated by the LiBiFood research group of the Universitat de Barcelona, following the procedure explained elsewhere (Bayés-García et al., 2016). All lipid extracts were stored in topaz vials with liquid nitrogen inert atmosphere in the freezer to avoid oxidation. 80 samples (20 samples for each category) were available. Before performing any analysis, samples were melted at 65 °C and homogenized by using a vortex.

Gas chromatography experiments were carried out to quantify the fatty acid moieties. The equipment consisted of a Shimadzu QP2010 coupled to a SGE BPX70 column (30 m x 0.25 mm, 0.25 μ m). The sample was diluted in n-hexane-dichloromethane (5:1) and carried with He. The injector temperature was 260 °C with split (split ratio 1:20). The mass spectroscopy coupled with the column worked with an ion injector temperature of 200 °C and an m/z range from 50.00 to 650.00.

DSC experiments were conducted for all samples (making a total of 80). They were carried out at atmospheric pressure using a PerkinElmer Diamond. Samples (9.0 – 9.9 mg) were weighted into 50 μ L aluminum pans, and covers were sealed into place. The instrument was calibrated with reference to the enthalpy and the melting points of indium (melting temperature 156.6 °C; $\Delta H = 28.45$ J/g) and decane (melting temperature -29.7 °C; $\Delta H = 202.1$ J/g) standards. An empty pan was used for reference. Dry nitrogen was used as purge gas in the differential scanning calorimetry (DSC) cell at 20 cm³/min. Thermograms were analyzed using Pyris Software to obtain the enthalpy (J/g, Integration of the DSC signals) and onset and end temperatures of the transformation (°C, intersection of the baseline and the initial and final tangents at the transformation). The thermal program used for all samples consisted of cooling from 65 °C to -80 °C at 2 °C/min followed by a subsequent heating process from -80 °C to 65 °C at a rate of 2 °C/min.

Three independent measurements were carried out when sufficient amount of sample was available. Then, random uncertainty was estimated with 95% threshold of reliability using the Student's method, which enables estimating the mean of normally distributed population when the population is small.

X-ray diffraction experiments, with both laboratory-scale and synchrotron radiation source, were performed for selected samples of each Iberian pig fat category. The X-ray diffraction results obtained by both laboratory-scale and synchrotron radiation source became equivalent. However, in this work we will show the synchrotron data for a better clarity and resolution. Laboratory-scale powder X-ray diffraction (lab-scale XRD) measurements were performed by using a PANalytical X'Pert Pro MPD powder diffractometer equipped with a hybrid Monochromator and an X'Celerator Detector. The equipment also included an Oxford Cryostream Plus 220 V (temperature 50-500 K). This diffractometer operates with Debye-Scherrer transmission. The sample was introduced in 1 mm-diameter Lindermann glass capillary that was rotated around its axis during the experiment to minimize preferential orientation of the crystallites. The step size was 0.013 °

from 1.004° to $28^\circ 2\theta$, and the measuring time was 2.5 minutes per pattern.

Synchrotron radiation X-ray diffraction (SR-XRD) experiments were conducted at the beamline BL11-NCD-SWEET of the Alba Synchrotron facility (Cerdanyola del Vallès, Spain) at 12.4 keV. The sample-detector distance was 2.2 m. X-ray scattering data were collected on a Quantum 210r ADSC detector with a pixel size of $102.4 \times 102.4 \mu\text{m}^2$ for small-angle X-ray diffraction (SAXD) data and on a LX255-HS Rayonix detector with a pixel size of $40 \times 40 \text{ mm}^2$ for the wide-angle X-ray diffraction (WAXD) data. The exposure time was 20 s. The temperature of the sample was controlled by a Linkam stage. SR-XRD patterns were acquired while the sample was cooled from 65 to -80°C and reheated to 65°C at the same controlled rate. The sample was placed in an aluminum sample cell with a Kapton film window. The q-axis calibration was obtained by measuring silver behenate for SAXD and Cr_2O_5 for WAXD. The software PyFAI was used to integrate the 2D WAXD into 1D data: the SAXD data were processed with in-house software.

3. RESULTS AND DISCUSSION

Figure 1 depicts the distribution of main fatty acids in lipid extracts corresponding to the four Iberian pig categories: *bellota* (*B*), *recebo* (*R*), *cebo de campo* (*CC*) and *cebo* (*C*).

The results showed that the main fatty acid was monounsaturated oleic acid (within the range 50-60%) for all categories, followed by saturated palmitic (17-24%) and stearic (7-12%) acids, diunsaturated linoleic acid (7-9%), monounsaturated palmitoleic acid (1-3%) and saturated miristic acid (1-2%). These results were in agreement with those reported by Diaz et al. (1996) and Gallardo et al. (2012) who defined POO, OOO, POL and POS as main triacylglycerol components of Iberian pig fat.

By comparing the lipid extracts compositions of the four categories, one may define a clear tendency which is related to the saturated/unsaturated nature of the three main fatty acids (oleic, palmitic and stearic). The percentage of unsaturated oleic acid decreased, whereas those of saturated palmitic and stearic increased in the sequence *bellota* (*B*) - *recebo* (*R*) - *cebo de campo* (*CC*) - *cebo* (*C*) as shown in Figure 1b.

Although some differences in fatty acid compositions were detected, these may not be determinant for a different crystallization and polymorphic behavior for the four Iberian pig categories. Variations in the polymorphic behavior may be mostly dictated by TAGs molecular structures (and resulting interactions), in which fatty acids can occupy different positions in the glycerol backbone.

The crystallization and polymorphic behavior of lipid extracts of *bellota*, *recebo*, *cebo de campo* and *cebo* categories were determined by DSC and XRD techniques when samples were cooled from 65°C to -80°C at a rate of $2^\circ\text{C}/\text{min}$ and subsequently heated in the same temperature range. Although DSC experiments were carried out for the 80 samples (20 samples for each category), cooling and heating curves of selected samples are shown in Figure 2. However, it is worth to mention that DSC curves corresponding to the same category became highly comparable.

All DSC thermograms consisted of four main thermal events: two exothermic peaks present in the cooling curves, and two main endothermic peaks in the heating curves. However, some differences were detected between the four categories, such as the occurrence of additional DSC signals or some shifting in temperatures at which phenomena occurred. In general terms, one may note that initial and end temperatures of crystallization in *bellota* and *recebo* samples (curves (1) and (2) in Figure 2a) were significantly lower than those of *cebo de campo* and *cebo* samples (curves (3) and (4)). Regarding the DSC heating curves, again *bellota* and *recebo* samples exhibited a similar thermal profile, characterized by the presence of two initial endothermic peaks with peak top temperatures between -20 and 0°C , and complex convoluted phenomena from 10 to 25°C . By contrast, the DSC heating curves corresponding to *cebo de campo* and *cebo* samples became less abrupt and continuous, as one may define just two main sharp endothermic peaks, with peak top temperatures at around 5 and 30°C (Figure 2b).

Then, due to the complexity of the DSC thermograms and the heterogeneity of some of the thermal events, we defined two main temperatures as indicators of the crystallization and melting behavior of the samples: the initial crystallization temperature, and end melting temperature. These temperatures may be also strongly

related to the fatty acid compositions of the lipid extracts. Figure 3 graphically shows onset crystallization and end melting temperatures for all the analyzed samples corresponding to each Iberian pig category (20 samples for each category).

The results indicated an average initial crystallization temperature of 8.6°C (with standard deviation of 1.6) and 9.6°C (standard deviation of 2.9) for the *bellota* and *recebo* samples, respectively. By contrast, *cebo de campo* and *cebo* samples exhibited higher onset crystallization temperatures of 15.9°C (standard deviation = 1.6) and 16.2°C (standard deviation = 3.1), respectively. Regarding the melting behavior, again comparable temperatures were detected in *bellota* and *recebo* samples, with average end temperatures of 28°C (standard deviation = 0.7) and 28.5°C (standard deviation = 1.2), respectively. As to *cebo de campo* and *cebo* categories, the corresponding average end melting temperature was 30.7 °C in both cases, with standard deviation of 0.9 and 1.0, respectively. From the results described above, one may note that two clear groups can be defined, in which crystallization and melting temperatures were significantly comparable: *bellota* - *recebo* and *cebo de campo* - *cebo*. As to standard deviation values, they were lower for melting temperatures, as can be observed by lower dispersion in temperature values in Figure 3. The different thermal behavior of the samples was interpreted by analyzing the crystallization and polymorphic behavior of selected samples for each category as will be described further on.

Figure 4 shows SR-SAXD and SR-WAXD data obtained when a *bellota* sample was cooled from 65°C to -80°C at a rate of 2°C/min and reheated to 65°C at the same rate.

During the cooling process, at a temperature of 6.3°C, the SR-SAXD pattern revealed the occurrence of a triple chain length structure (3L) peak at 3.5 nm. Simultaneously, in the SR-WAXD pattern, typical β' peaks at 0.41 and 0.38 nm were detected. Then, this crystallization process corresponded to a β' -3L form and caused the first exothermic DSC peak occurring at around 8°C (peak top temperature, see Figure 2a - curve (1)). At -15.5°C, a double chain length structure peak (2L) at 4.3 nm appeared in the SR-SAXD pattern accompanied by a SR-WAXD peak at 0.39 nm, which may correspond to a β' -2L form crystallization. This crystallization process may be attributable to the exothermic peak with peak top temperature at around -10°C (Figure 2a - curve (1)). On further cooling, at -21.5°C, two extra SR-WAXD peaks occurred at 0.42 and 0.41 nm, probably due to the crystallization of an additional β' -2L polymorphic form. This phenomenon may correspond to the last DSC peak at -21°C observed when cooling. During the subsequent heating process, at -2.5°C, the β' -2L form peaks at 0.42, 0.41 and 0.39 nm vanished, while the intensity of the 2L peak at 4.3 nm considerably decreased. This SR-SAXD peak completely disappeared at 5.4 °C. This changes may be due to the melting process of the two β' -2L forms previously crystallized, and they may correspond to the two broad endothermic DSC peaks with maximum temperatures of -12 and 0°C. On further heating, at 17.4°C, the SR-SAXD peak at 3.5 nm vanished, together with the SR-WAXD peaks at 0.41 and 0.38 nm, due to the melting of the β' -3L form. Soon after, new peaks at 4.4 and 0.46 nm occurred, which may correspond to a newly-formed most stable β -2L polymorph, probably through melt-mediation after the melting of β' -2L forms. This most stable form finally melted at around 39.2°C (see enlarged figure in Figure 4), temperature at which no peaks were present in the SR-XRD patterns, that is in accordance with the corresponding DSC thermograms. One may note the presence of a last and very flat endothermic signal in the corresponding DSC thermogram (see curve (1) in Figure 2b), which is related to the melting of this most stable β -2L form.

The polymorphic behavior of *recebo* samples was highly similar to that of *bellota* samples, as shown in Figure 5.

By cooling the molten *recebo* sample at a rate of 2°C/min, triple chain length structure peak at 3.5 nm (SR-SAXD) and short spacing values of 0.41 and 0.38 nm (SR-WAXD) occurred at 2.4°C, corresponding to the crystallization of a β' -3L form. This event may correspond to the exothermic DSC signal with peak top temperature of 5°C (see Figure 2a). On further cooling, at -21.4°C, a 2L structure peak at 4.3 nm was observed in the SR-SAXD pattern and, simultaneously, β' WAXD peaks at 0.44, 0.43 and 0.39 nm were detected (β' -2L form crystallization). Finally, at a lower temperature of -27.5°C, an additional peak at 0.42 nm appeared, which most probably corresponded to the crystallization of another β' -2L form. These crystallization processes of β' -2L forms may be attributable to the exothermic DSC events with maximum

temperatures of -12 and -25°C of the related cooling thermogram (see curve (2) in Figure 2a). As to the heating step, when completely crystallized *recebo* sample was heated at 2°C/min, the first observable change took place at 5.4°C, temperature at which a β' -2L form melted (vanishing of the SR-WAXD peaks at 0.44, 0.43 and 0.39 nm and decrease of the intensity of the SR-WAXD peak at 4.3 nm). Within the temperature range from 11.4 to 17.3°C, all the SR-XRD peaks vanished, so that one may deduce that β' -2L and β' -3L forms melted. Soon after, new SR-SAXD peak at 4.4 nm appeared (see enlarged figure in Figure 5) and, simultaneously, typical β SR-WAXD peak was observed at 0.46 nm. Then, one may conclude that, similarly to the *bellota* sample case, melt-mediated transformation occurred to obtain most stable β -2L form, which finally melted at around 35.2°C (see very flat endothermic DSC peak with peak top temperature of about 35 °C in curve (2) of Figure 2b). *Recebo* sample exhibited, therefore, a very similar polymorphic behavior to that of *bellota*. However, crystallization and melting temperatures were lower in *recebo* than in *bellota* in this specific case, which is in accordance with the dispersion in crystallization and melting temperatures determined in the characterized *recebo* samples (see Figure 3).

Different crystallization and polymorphic behavior was detected in the *cebo de campo* and *cebo* samples. Figure 6 shows the SR-XRD data corresponding to *cebo de campo*, which allowed the identification of the thermal phenomena observed by DSC (curve (3) in Figure 2).

When cooled, an initial concurrent crystallization of β' -2L and β' -3L forms was detected at 16.3 °C. These events were related to the DSC exothermic peak with maximum temperature of 13 °C. These forms were identified by long spacing values of 4.9 and 3.5 nm, respectively, and short spacing values of 0.41 and 0.38 nm. On further cooling, at -11.5 °C, the SR-SAXD pattern showed the occurrence of an additional 2L peak at 4.3 nm and, at -15.5 °C, the SR-WAXD pattern exhibited two new peaks at 0.43 and 0.39 nm, which may refer to the formation of an additional β' -2L form or two additional β' -2L forms, as will be justified through the heating step. Regarding the DSC cooling thermogram, these phenomena may correspond to the second main exothermic peak with peak top temperature at around -10 °C. During the heating process, the first observable change took place at 3.5 °C, when the 0.39 nm peak disappeared, due to the melting of one of the newly-formed β' -2L forms (on the DSC heating thermogram, this process was related to the endothermic event with $T_{\max} = 2$ °C). At 25.3 °C, the 4.9 nm peak disappeared, at 27.3 °C, the peaks at 0.43, 0.41 and 0.38 nm also vanished and, soon after, at 31.3 °C, the peak at 3.5 nm also disappeared. These phenomena corresponded to the melting of the remaining β' -2L forms and β' -3L form. Then, at 33.2 °C, the peak at 4.3 nm vanished and a new peak at 4.4 nm occurred in the SR-SAXD pattern, together with a SR-WAXD peak at 0.46 nm, indicating the crystallization of a most stable β -2L form, most probably through a melt-mediated process. Finally, at a temperature of 43.2 °C, no SR-XRD peaks were present, and the melting of most stable β -2L form may be related to the flat endothermic DSC peak with maximum temperature of around 40 °C, observable in curve (3) of Figure 2b.

A *cebo* sample was subjected to the same thermal treatment and the SR-XRD pattern obtained are shown in Figure 7.

When cooled from 65 °C to -80 °C at a rate of 2 °C/min, the SR-SAXD pattern exhibited, at 13.4 °C, the occurrence of an initial peak at 4.8 nm (2L) and, simultaneously, the SR-WAXD pattern showed the formation of typical β' form peaks at 0.41 and 0.38 nm (β' -2L form crystallization). Soon after, at 11.3 °C, a SR-SAXD peak at 3.4 nm (3L) accompanied by SR-WAXD peaks at 0.43 and 0.38 nm were detected, due to the crystallization of a β' -3L polymorph. These two crystallization processes (β' -2L and β' -3L forms) may be related to the first observable exothermic DSC peak with peak top temperature of about 17 °C (curve (4) in Figure 2a). Then, at -14.5 °C, an additional β' -2L form crystallized, with long and short spacing values of 4.3 and 0.39 nm. This last event may correspond to the DSC exothermic peak at $T_{\max} = -9$ °C. Finally, at -24.4 °C, the SR-WAXD pattern indicated the occurrence of a β' form peak at 0.42 nm (observed on the DSC cooling curve at $T_{\max} = -23$ °C). Nevertheless, the chain length structure of this newly formed polymorph could not be determined due to the overlapping of the peaks. During the subsequent heating stage, the first melting phenomenon corresponded to the lastly formed β' -2L form and it was observed at 9.4 °C, temperature at which the SR-WAXD peak at 0.39 nm vanished and the intensity of the SR-SAXD

peak at 4.3 nm decreased significantly. This event may be related to the first important endothermic DSC signal with peak top temperature of around 4 °C. According to the SR-XRD data, at 27.3 °C, the initially formed β' -2L form and the β' form with no definite long spacing value melted (peaks at 4.8, 0.42, 0.41 and 0.38 nm). Later, at 29.3 °C, the peak at 3.5 nm disappeared, which may be attributed to the melting of β' -3L form. These melting processes were attributed to the second main endothermic signals with maximum temperature of about 29 °C. Further on, and similarly to other Iberian categories, at 35.2 °C, most stable β -2L form occurred, with long and short spacing values of 4.4 nm and 0.46 nm, respectively. Finally, this most stable form melted at 45.2 °C, temperature at which no peaks were present. In the case of *cebo* sample, the last flat endothermic DSC peak with maximum temperature of about 40 °C, which may correspond to the melting of most stable β -2L form, becomes more pronounced than for other categories.

The polymorphic behavior of the *cebo de campo* and *cebo* samples became highly similar, as will be discussed further on. Moreover, both crystallization and melting temperatures became comparable.

All samples of lipid extracts belonging to the different Iberian pig categories of *bellota*, *recebo*, *cebo de campo* and *cebo* exhibited highly complex polymorphic behavior at the experimental conditions examined. This complexity was detected in the corresponding DSC cooling and heating thermograms, but also in the SR-XRD patterns. As to the thermal behavior of the samples, the occurrence of overlapped endothermic and exothermic DSC phenomena predominated, often taking place continuously throughout all the thermal treatment applied. The same happened with SR-XRD data, in which concurrent crystallization of multiple polymorphic forms with similar short-spacing values created significant difficulties in the identification of polymorphic forms. However, SR-SAXD patterns facilitated this task.

As a summary, Figure 8 depicts the polymorphic behavior determined for the four Iberian pig categories.

SR-XRD data confirmed the tendencies observed by the DSC thermograms of the samples (see Figures 2 and 3). The four Iberian pig categories could be arranged in two main groups: that formed by the *bellota* and *recebo* categories, and that constituted by the *cebo de campo* and *cebo* categories. *Bellota* and *recebo* samples exhibited a simpler polymorphic behavior compared to that of *cebo de campo* and *cebo*. When the two samples were cooled from the molten state, three different polymorphic forms crystallized: an initial β' -3L form followed by two different β' -2L forms. Then, when heated, these forms melted, and some fraction of the liquid crystallized to obtain most stable β -2L form, which finally melted at a temperature of about 35-40 °C. By contrast, *cebo de campo* and *cebo* samples crystallized in a higher number of polymorphic forms. The first characteristic event was the initial crystallization of a β' -2L form with a long spacing value of 4.8 or 4.9 nm, which was not detected in *bellota* and *recebo* samples. This crystallization was followed by the occurrence of a β' -3L form and at least two more β' -2L forms. When samples were heated, and similarly to the *bellota* - *recebo* case, these polymorphic forms melted and some liquid fraction re-crystallized to obtain most stable β -2L form through melt-mediation. This most stable form melted at around 43-45 °C, temperature significantly higher than that corresponding to *bellota* and *recebo* samples. Higher crystallization and melting temperatures in *cebo de campo* and *cebo* samples compared to *bellota* and *recebo* was another distinctive characteristic previously confirmed by DSC data, as shown in Figures 2 and 3. Furthermore, in general *bellota* and *recebo* categories exhibited sharper and better-defined exothermic and endothermic signals, whereas the phenomena showed by *cebo de campo* and *cebo* categories became more continuous through all the thermal program applied due to the occurrence of a higher number of polymorphic forms which may be overlapping. The higher crystallization and melting temperatures detected in *cebo de campo* and *cebo* categories may be related to a more saturated composition of fatty acid moieties, as confirmed by chromatographic techniques (see Figure 1).

By considering the characteristics that define each Iberian pig category, regarding the feeding system during the fattening phase (consumption of acorns and/or concentrated feed), grazing (that is, doing physical exercise), etc., one may extract some conclusions about which are the driving factors that determine the polymorphic behavior of their lipid extracts. Figure 9 summarizes these distinctive characteristics associated to the rearing system and grazing for the four categories.

The results presented in this work demonstrated that *bellota* and *recebo* samples exhibited essentially the same polymorphic behavior, and the same occurred to *cebo de campo* and *cebo* categories. As shown in Figure 9, distinctive characteristics of both *bellota* and *recebo* are the consumption of acorns and grazing, which involves exercise. Grazing becomes another characteristic activity of *cebo de campo*, similarly to the commercial feed consumption, which is common in *recebo*, *cebo de campo* and *cebo* categories. Thus, one may conclude that the key factor which determines the polymorphic behavior of Iberian pig lipid extracts is not the physical exercise practiced by the pig, but the inclusion of acorns in the feeding system. In this sense, the polymorphic behavior may be used as a tool to discriminate among some of the Iberian pig categories. In our previous work (Bayés-García et al. 2016) we concluded that both DSC and XRD techniques could be used as identification tools to discriminate between the two most differentiated categories: *bellota* and *cebo* categories. With the present work we showed that it is also possible to discriminate among intermediate categories of *recebo* and *cebo de campo*, as *recebo* samples exhibit an equivalent behavior to that of *bellota*, whereas *cebo de campo* becomes highly similar to *cebo*. Although further work is needed to analyze a higher number of samples of all categories in order to confirm the results presented here, this work becomes a good approach to show the potential of polymorphic tools to be used as a fingerprint for the discrimination among different product categories and, therefore, to combat food fraud.

4. CONCLUSIONS

DSC and XRD techniques (with both laboratory-scale and synchrotron radiation source) were used to authenticate among different categories of Iberian pig lipid extracts. Lower amount of polymorphic forms occurred in *bellota* and *recebo* samples compared to *cebo de campo* and *cebo*. Furthermore, the more unsaturated fatty acids composition of *bellota* and *recebo* categories resulted in lower crystallization and melting temperatures, compared to *cebo de campo* and *cebo*. By considering the differences in rearing systems of pigs belonging to the different categories, we concluded that the key factor which determined the polymorphic behavior of Iberian pig lipid extracts was not the physical exercise practiced by the pig, but the inclusion of acorns in the feeding system. Although further work is needed to analyze a higher number of samples of all categories to confirm the results presented, with this work we showed that crystallographic techniques, such as DSC and XRD, may be promoted to be used as fingerprinting tools for food products authentication.

ACKNOWLEDGEMENTS

The authors would like to thank the financial support of the Ministerio de Economía y Competitividad through Project No. MAT2015-65756-R. Funding from the Alba synchrotron facility for performing SR-XRD experiments is gratefully appreciated. SR-XRD experiments were conducted with the approval of the Alba Scientific Advisory Committee (Proposal No. 2014070991). The authors thank Dr. Marc Malfois, responsible for BL11-NCD-SWEET at Alba, for his help. They also acknowledge Dr. Juan M. García-Casco from the Instituto Nacional de Investigación y Tecnología Agraria y Alimentaria (INIA) for providing the Iberian pig fat samples.

REFERENCES

- Arce, L.; Domínguez-Vidal, A.; Rodríguez-Estévez, V.; López-Vidal, S.; Ayora-Cañada, M. J.; Valcárcel, M. (2009). Feasibility study on the use of infrared spectroscopy for the direct authentication of Iberian pig fattening diet. *Analytica Chimica Acta*, **636**: 183-189.
- Bayés-García, L.; Tres, A.; Vichi, S.; Calvet, T.; Cuevas-Diarte, M. A.; Codony, R.; Boatella, J.; Caixach, J.; Ueno, S.; Guardiola, F. (2016). Authentication of Iberian dry-cured ham: New approaches by polymorphic fingerprint and ultrahigh resolution mass spectrometry. *Food Control*, **60**: 370-377.
- Bayés-García, L.; Sato, K.; Ueno, S. (2020). Polymorphism of Triacylglycerols and Natural Fats, In Bailey's Industrial Oil and Fat Products, Hoboken. United States: Wiley.
- Campos, R.; Narine, S. S.; Marangoni, A. G. (2002). Effect of cooling rate on the structure and mechanical properties of milk fat and lard. *Food Research International*, **35**: 971-981.

Chiavaro, E.; Rodriguez-Estrada, M. T.; Barnaba, C.; Vittadini, E.; Cerretani, L.; Bendini, A. (2008a). Differential scanning calorimetry: A potential tool for discrimination of olive oil commercial categories. *Analytica Chimica Acta* , **625** : 215-226.

Chiavaro, E.; Vittadini, E.; Rodriguez-Estrada, M. T.; Cerretani, L.; Bendini, A. (2008b). Differential scanning calorimeter application to the detection of refined hazelnut oil in extra virgin olive oil. *Food Chemistry* , **110** : 248-256.

Cordella, C.; Moussa, I.; Martel, A. C.; Sbirrazzuoli, N.; Lizzani-Cuvelier, L. (2002). Recent developments in food characterization and adulteration detection: Techniques-oriented perspectives. *Journal of Agricultural and Food Chemistry* , **50** : 1751-1764.

Davenel, A.; Riaublanc, A.; Marchal, P.; Gandemer, G. (1999). Quality of pig adipose tissue: relationship between solid fat content and lipid composition. *Meat Science* , **51** : 73-79.

Diaz, I.; García Regueiro, J. A.; Casillas, M.; De Pedro, E. (1996). Triglyceride composition of fresh ham fat from Iberian pigs produced with different systems of animal nutrition. *Food Chemistry* , **55** : 383-387.

Ellis, D. I.; Brewster, V. L.; Dunn, W. B.; Allwood, J. W.; Golovanov, A. P.; Goodacre, R. (2012). Fingerprinting food: current technologies for the detection of food adulteration and contamination. *Chemical Society Reviews* , **41** : 5706-5727.

Gallardo, E.; Narváez-Rivas, M.; Pablos, F.; Jurado, J. M.; León-Camacho, M. (2012). Subcutaneous fat triacylglycerols profile from Iberian pigs as a tool to differentiate between intensive and extensive fattening systems. *Journal of Agricultural and Food Chemistry* , **60** : 1645-1651.

González-Martin, I.; González-Pérez, C.; Hernández Méndez, J.; Marqués-Macias, E.; Sanz Poveda, F. (1999). Use of isotope analysis to characterize meat from Iberian-breed swine. *Meat Science* , **52** : 437-441.

Larsson, K., Quinn, P., Sato, K., & Tiberg, F. (2006). *Lipids: Structure, physical properties and functionality*, Bridgwater, England: The Oily Press.

Motoyama, M.; Ando, M.; Sasaki, K.; Hamaguchi, H. (2010). Differentiation of Animal Fats from Different Origins: Use of Polymorphic Features Detected by Raman Spectroscopy. *Applied Spectroscopy* , **64** : 1244-1250.

Motoyama, M.; Chikuni, K.; Narita, T.; Aikawa, K.; Sasaki, K. (2013). In situ Raman spectrometric analysis of crystallinity and crystal polymorphism of fat in porcine adipose tissue. *Journal of Agricultural and Food Chemistry* , **61** : 69-75.

Narváez-Rivas, M.; Rios, J. J.; Arteaga, J. F.; Quilez, J. F.; Barrero, A. F.; León-Camacho, M. (2008). Determination of ent-kaurene in subcutaneous fat of Iberian pigs by gas chromatography multi-stage mass spectrometry with the aim to differentiate between intensive and extensive fattening systems. *Analytica Chimica Acta* , **624** : 107-112.

Narváez-Rivas, M.; Pablos, F.; Jurado, J. M.; León-Camacho, M. (2011). Authentication of fattening diet of Iberian pigs according to their volatile compounds profiles from raw subcutaneous fat. *Analytical and Bioanalytical Chemistry* , **399** : 2115-2122.

Petrón, M. J.; Muriel, E.; Timón, M. L.; Martín, L.; Antequera, T. (2004). Fatty acids and triacylglycerols profiles from different types of Iberian dry-cured hams. *Meat Science* , **68** : 71-77.

Royal Decree 4/2014. Approves the quality standards for the Iberian meat, ham, shoulders and loin (pp. 1569-1585). BOE, No. 10 (January 11th, 2014).

Ruiz, J.; Cava, R.; Antequera, T.; Martín, L.; Ventanas, J.; López-Bote, J. (1998). Prediction of the feeding background of Iberian pigs using the fatty acid profile of subcutaneous, muscle and hepatic fat. *Meat Science* , **49** : 155-163.

Svenstrup, G.; Brüggemann, D.; Kristensen, L.; Risbo, J.; Skibsted, L. H. (2005). The influence of pretreatment on pork fat crystallization. *European Journal of Lipid Science and Technology*, **107** : 607-615.

Tejeda, J. F.; Gandemer, G.; Antequera, T.; Viau, M.; García, C. (2002). Lipid traits of muscles as related to genotype and fattening diet in Iberian pigs: total intramuscular lipids and triacylglycerols. *Meat Science* , **60** : 357-363.

Timón, M. L. ; Ventanas, J.; Carrapiso, A. I.; Jurado, A.; García, C. (2001). Subcutaneous and intermuscular fat characterization of dry-cured Iberian hams. *Meat Science* , **58** : 85-91.

Viera-Alcaide, I.; Vicario, I. M.; Escudero-Gilete, M. L.; Graciani Constante, E.; León-Camacho, M. (2008). A multivariate study of the triacylglycerols composition of the subcutaneous adipose tissue of Iberian pig in relation to the fattening diet and genotype. *Grasas y Aceites* , **59** : 327-336.

TABLES

Table 1. Characteristics of final period of fattening phase of Iberian pig categories

| Iberian pig category | Feeding system | Minimum duration of <i>montanera</i> |
|----------------------|--|--------------------------------------|
| <i>Bellota</i> | Acorns, grass, other natural resources | 60 |
| <i>Recebo</i> | Acorns, grass, other natural resources, commercial feeds | 60 |
| <i>Cebo de campo</i> | Commercial feeds (mainly) | 60 |
| <i>Cebo</i> | Commercial feeds | — |

FIGURE LEGENDS

Figure 1. a) Fatty acids distribution per weight (%) of lipid extracts of *bellota* (*B*), *recebo* (*R*), *cebo de campo* (*CC*) and *cebo* (*C*) samples. b) Evolution in oleic, palmitic and stearic acids.

Figure 2. DSC cooling (a) and subsequent heating (b) thermograms of *bellota* (1), *recebo* (2), *cebo de campo* (3) and *cebo* (4) samples when cooled from 65 °C to -80 °C at 2 °C/min and heated to 65 °C at the same rate.

Figure 3. Onset crystallization (a) and end melting (b) temperatures of eighty samples of Iberian pig lipid extracts of *bellota* (*B*), *recebo* (*R*), *cebo de campo* (*CC*) and *cebo* (*C*) samples.

Figure 4. SR-SAXD (a) and SR-WAXD (b) patterns obtained when *bellota* sample was cooled from 65 °C to -80 °C at 2 °C/min and reheated to 65 °C at the same rate.

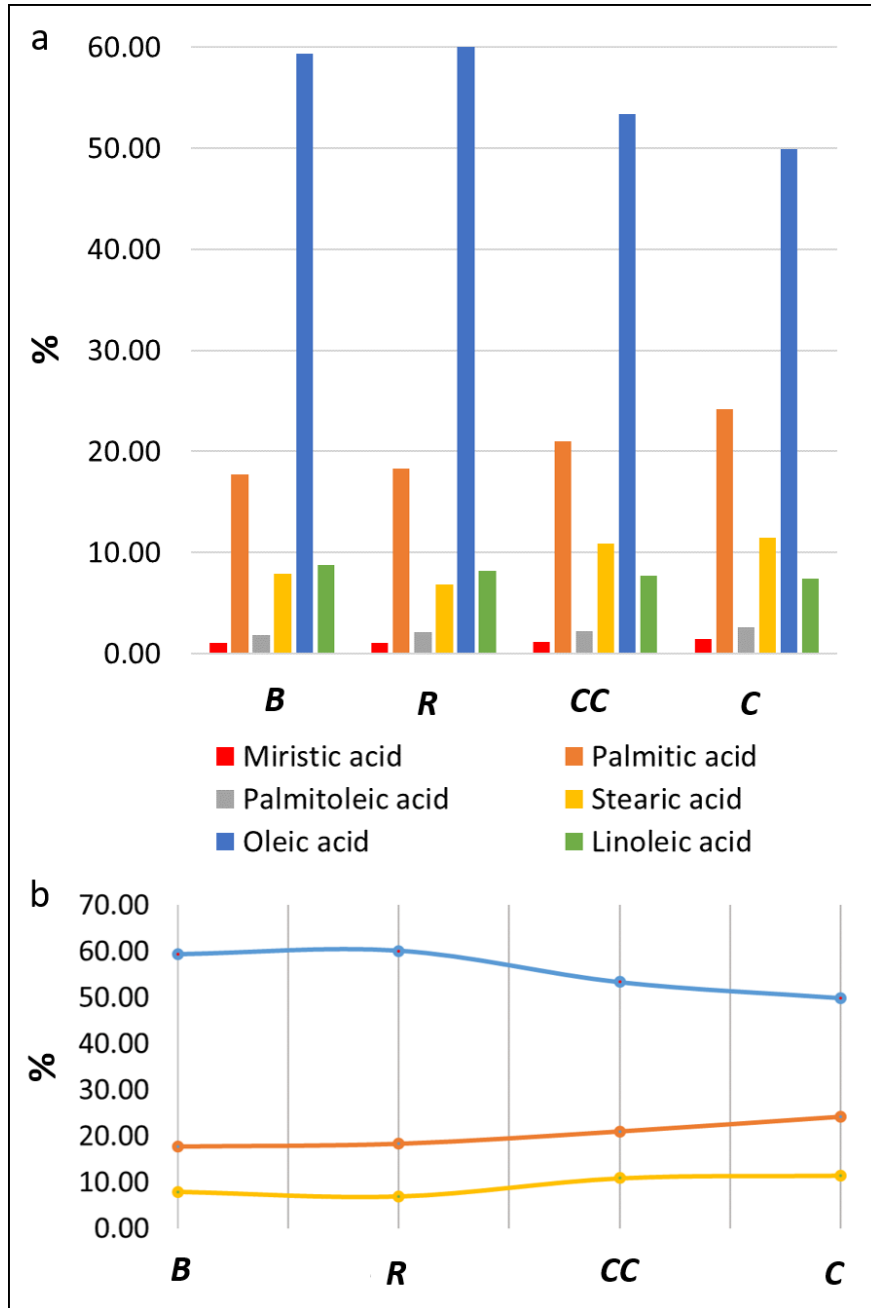
Figure 5. SR-SAXD (a) and SR-WAXD (b) patterns obtained when *recebo* sample was cooled from 65 °C to -80 °C at 2 °C/min and reheated to 65 °C at the same rate.

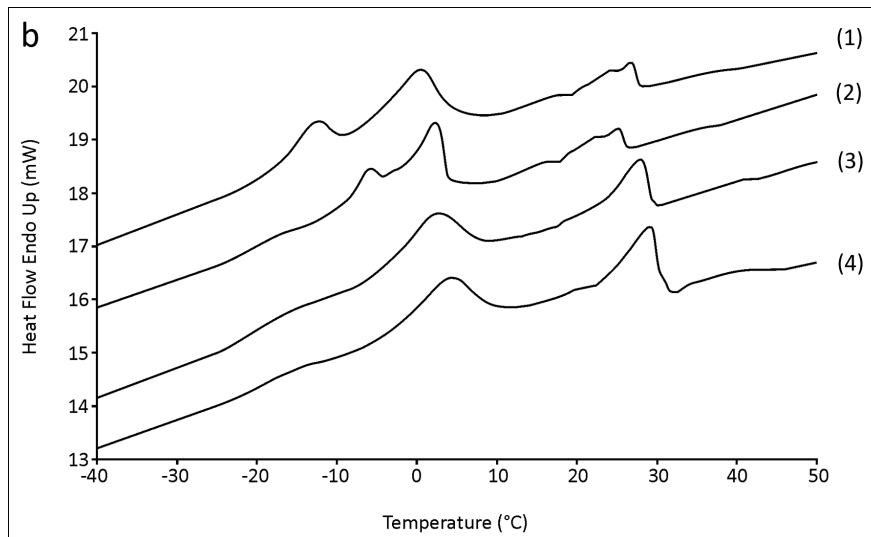
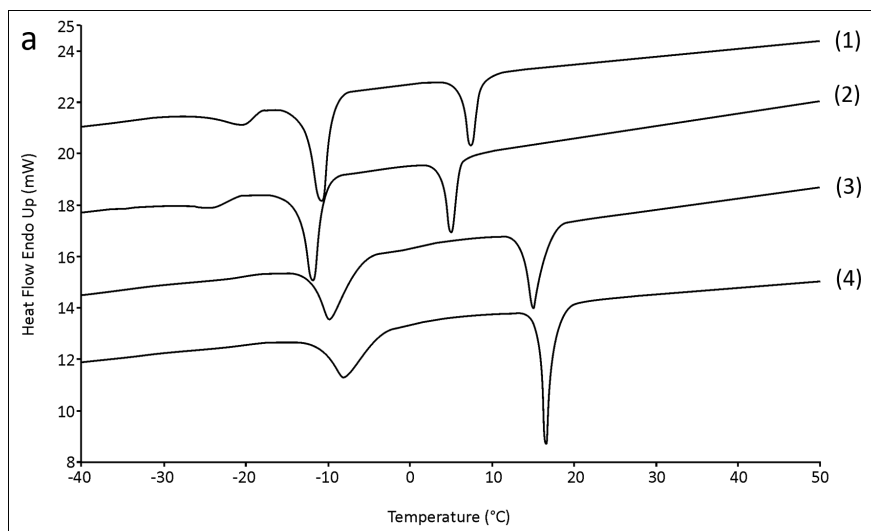
Figure 6. SR-SAXD (a) and SR-WAXD (b) patterns obtained when *cebo de campo* sample was cooled from 65 °C to -80 °C at 2 °C/min and reheated to 65 °C at the same rate.

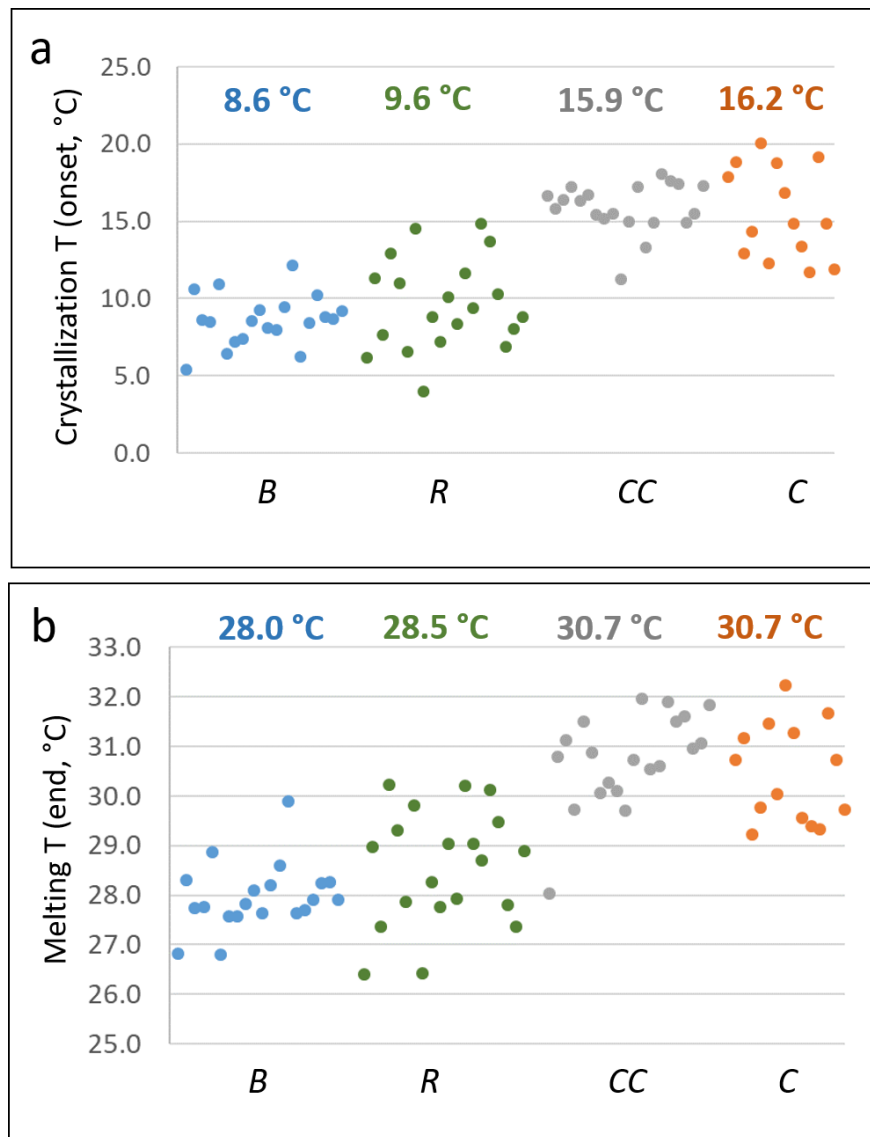
Figure 7. SR-SAXD (a) and SR-WAXD (b) patterns obtained when *cebo* sample was cooled from 65 °C to -80 °C at 2 °C/min and reheated to 65 °C at the same rate.

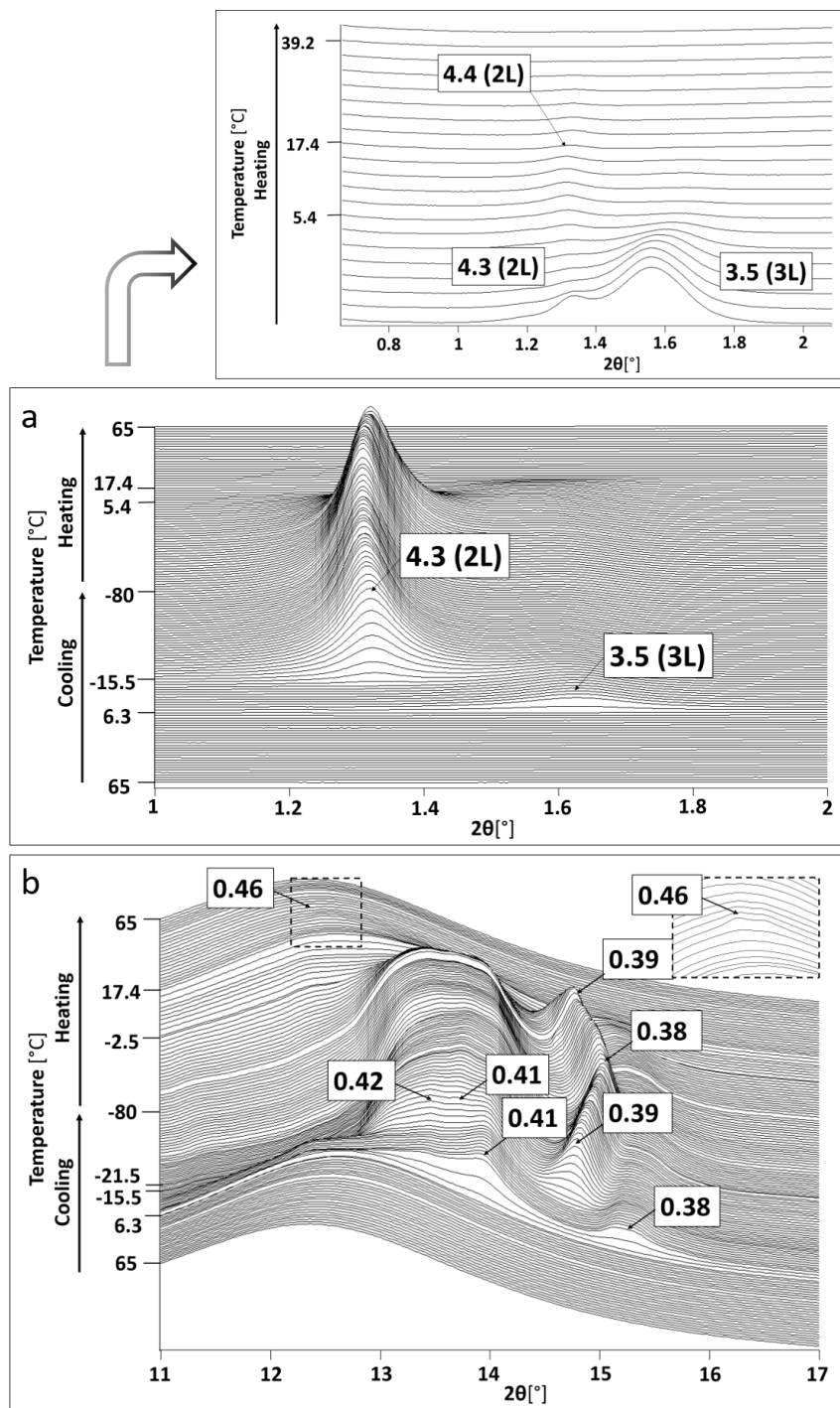
Figure 8. Polymorphic crystallization and transformation of Iberian pig categories.

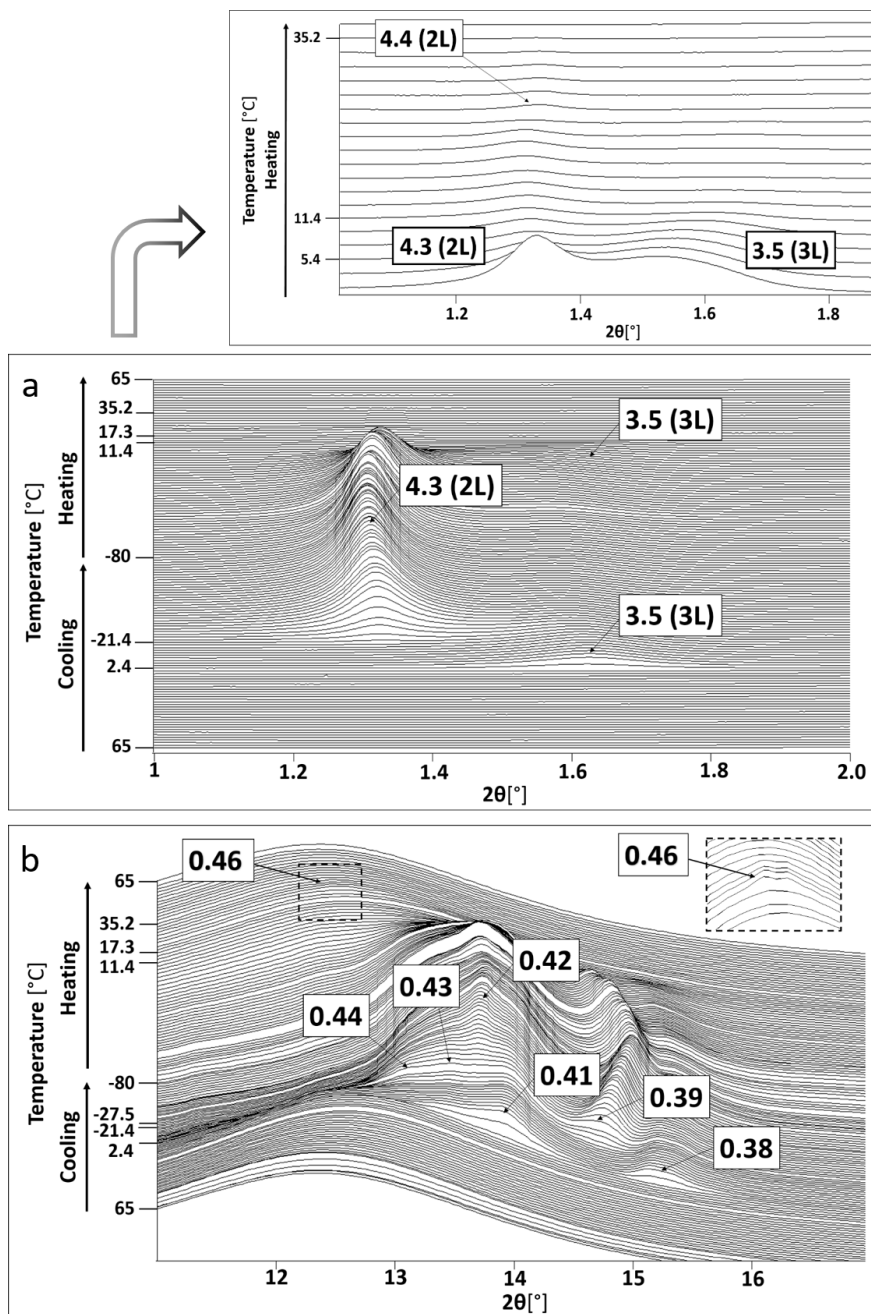
Figure 9. Summary of the characteristics of the different rearing systems of Iberian pigs.

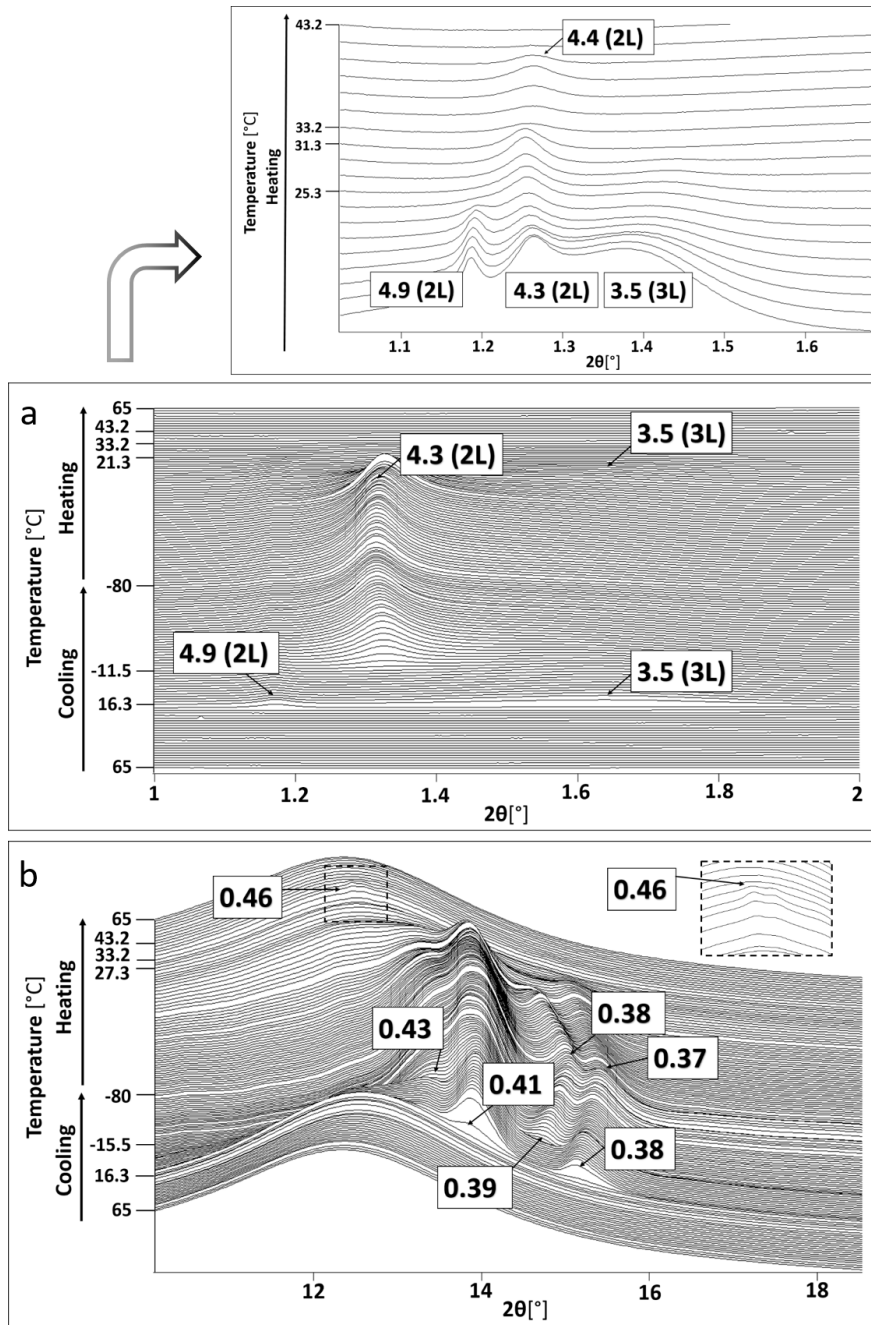


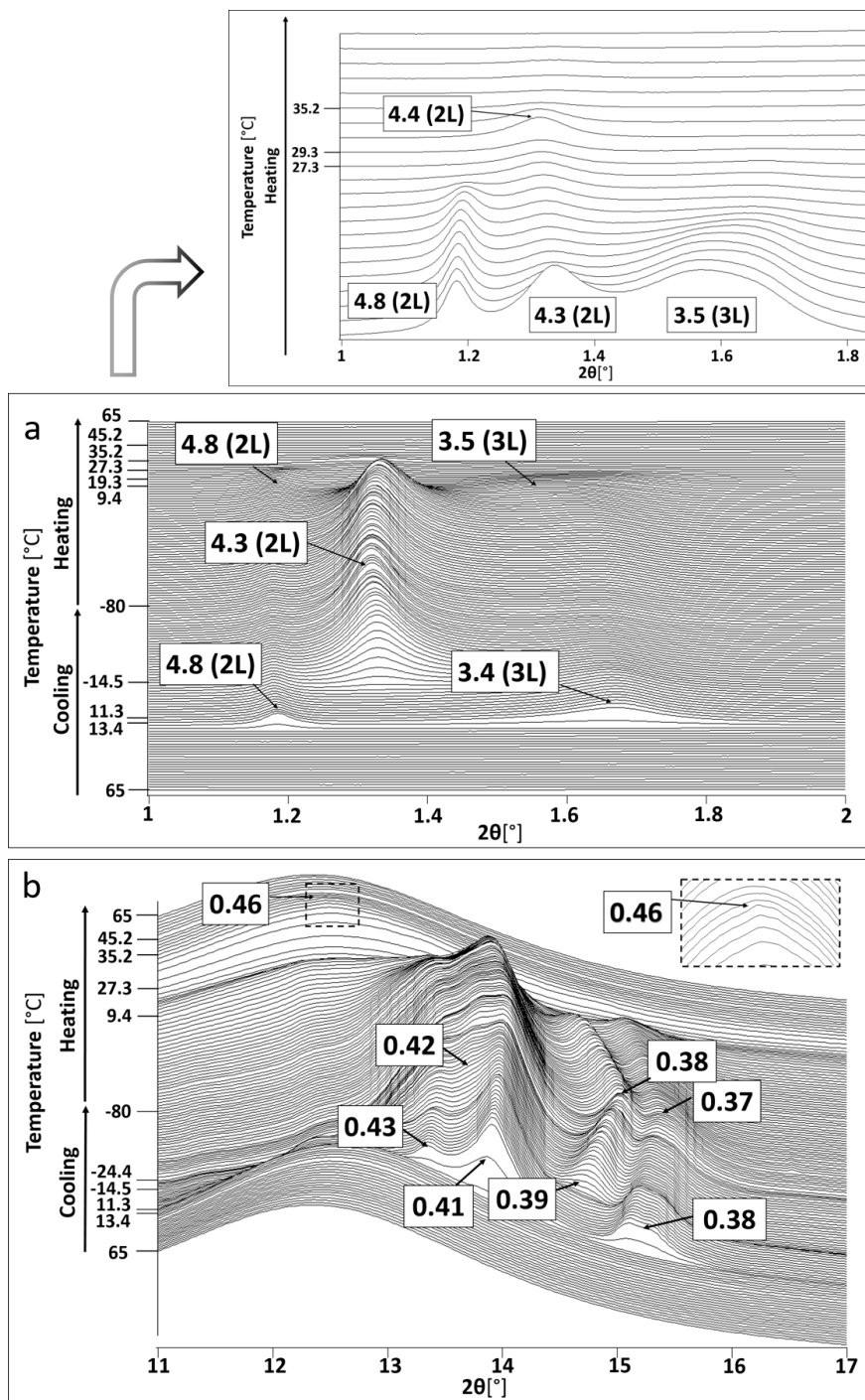


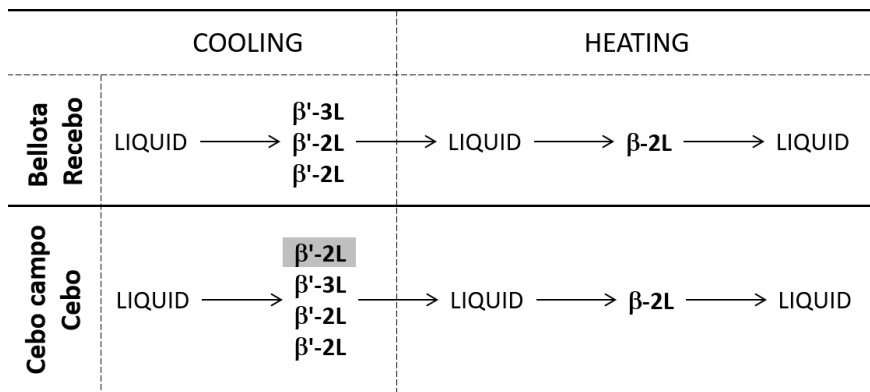












| Iberian pork category | Acorns consumption | Commercial feed consumption | Physical exercise (grazing) |
|-----------------------|--------------------|-----------------------------|-----------------------------|
| Bellota | ✓ | X | ✓ |
| Recebo | ✓ | ✓ | ✓ |
| Cebo de campo | X | ✓ | ✓ |
| Cebo | X | ✓ | X |